A NEW RADIUS-LUMINOSITY RELATION:
USING THE NEAR-INFRARED CaII TRIPLET

M. L. MARTÍNEZ-ALDAMA, S. PANDA and B. CZERNY

Center for Theoretical Physics, Polish Academy of Sciences,
Al. Lotników 32/46, 02-668 Warsaw, Poland
E–mail: mmary@cft.edu.pl

Abstract. The Radius-Luminosity (RL) relation has been an excellent option to estimate the black hole mass in single-epoch observations. However, the inclusion of sources radiating close to the Eddington limit show a departure from the standard RL relation, bringing into discussion the validity of this relation for the general AGN population. Since the accretion rate seems to be the main driver behind this scatter, corrections based on it have been suggested to recover the predicted time delay. However, there is a need to search for independent observables that, when incorporated as a correction, can recover the classical result. Particularly, the Eigenvector 1 scheme has found that the intensity of the very low–ionization lines such as the optical Fe II and the Near–Infrared (NIR) Ca II triplet are driven by the Eddington ratio. A correction based on the optical Fe II has recovered the classical RL relation. Combining the aforementioned deductions, this contribution presents a correction based on the NIR Ca II triplet. The correction is computed in two ways: (1) using the linear relation between Fe II and Ca II using 75 objects, and (2) considering independent measurements of Ca II in 13 sources with existing reverberation mapping measurements. The first case provides similar results to one obtained with Fe II. In the second case, the limited sample affects the recovery of a good correction. These results show the relevance and the potential use of the Ca II ion, which should be considered for future observational programs.

1. INTRODUCTION

The distance determination in the Universe is crucial for cosmological studies. Active Galactic Nuclei (AGNs) have been detected in the high-redshift Universe ($z \sim 7.4$, Onoue et al. 2020) enabling their use as potential standard candles. Some observational properties of AGNs have been identified with this purpose (Risaliti & Lusso et al. 2019, Dultzin et al. 2020). However, the uncertainties associated with the cosmological estimations are still high compared to the ones shown by Cepheids, SNIa (Riess et al. 2018) or Cosmic Microwave Radiation (Planck Collaboration et al., 2020). In order to improve the existing measurements using AGNs, we need to perform a better determination of the their properties.

A solid relation between the broad line region (BLR) properties and the Eddington ratio (L_{bol}/L_{Edd}) has been revealed by the Eigenvector 1 scheme (Boroson and Green 1992, Marziani et al. 2003, Shen and Ho 2014, Panda et al. 2018). Usually, high

Eddington objects show signatures of outflows and low equivalent widths in high ionization lines (e.g. C IVλ1549 or Si IV λ1397), tiny narrow emission lines (e.g. [O III] $\lambda\lambda$5007, 4959) and a strong contribution of the very low–emission lines such as the optical Fe II and the NIR Ca II triplet. In addition, highly accreting objects show a small variability in the photometric properties (Sanchez et al. 2017, Zajaček et al. 2021).

In the past, super-Eddington sources were not preferentially monitored by reverberation mapping studies. Since a long monitoring time with decent cadence is required for the reverberation mapping technique, objects with strong [O III] $\lambda\lambda$5007, 4959 were selected to be observed by small ground-based telescopes in moderate timescales and to ensure correct flux normalizations (Peterson et al. 1998). Thus, the Radius-Luminosity (RL) relation was mostly populated with objects with small Eddington ratios. Recently, the inclusion of highly accreting objects carried out by the Super-Eddington Accreting Massive Black Holes (SEAMBHs) project (Du et al. 2018 and references therein) reveals that these AGN population show a departure from the classic RL relation, which directly affects the black hole mass determination in single-epoch measurements. Since the departure seems to be related to the Eddington ratio, some corrections have been proposed to recover the predicted time delay (Du et al. 2015, Martínez-Aldama et al. 2019, Du & Wang 2019, Dalla Bontà et al 2020, Fonseca-Alvarez et al. 2020, Martínez-Aldama et al. 2020). However, due to the self-dependence between the determination of the Eddington ratio and the time delay, the best option is to select independent observational properties, which in turn are correlated with the Eddington ratio. The most natural parameter is the strength of the optical Fe II expressed as the R_{FeII} (Fe II/Hβ). So, including R_{FeII} in a multilinear fitting with the luminosity and the time delay (τ_{obs}), Du and Wang (2019) and Yu et al. (2019) obtained similar results to the one estimated by the classical the RL relation (Bentz et al. 2013).

On the other hand, the NIR Ca II triplet λ8498, λ8542, λ8662 (hereafter CaT) has a linear relation with the optical Fe II (Persson 1988, Joly 1989, Martínez-Aldama et al. 2015, Marinello et al. 2016, Panda et al. 2020). The relation between the two parameters can be expressed as follow (Panda et al. 2020):

$$\log R_{CaT} \approx (0.974 \pm 0.119) \log R_{FeII} - (0.657 \pm 0.041), \tag{1}$$

where R_{CaT} is the flux ratio Ca II/Hβ, which is in turn related to the Eddington ratio (Martínez–Aldama et al. 2021). Contrary to the Fe II, the CaT is a simpler ionic species and the photoionization codes can reproduce its behavior in a better way (Ferland & Persson, 1989; Panda et al. 2020, 2021). However, observing the CaT in AGN at intermediate and high redshifts is a challenge due to the presence of the telluric bands in the near- and mid-infrared. The upcoming generation of space observatories and the improvement in detectors mounted on ground-based telescopes will offer a good possibility to observe the CaT in the future.

In this contribution, we explore a multilinear RL relation where R_{CaT} is included with the purpose to correct the RL relation by the accretion rate effect. The samples and methods are summarized in Sec. 2. The multilinear RL relations are described in Sec. 3. Finally, discussions and conclusions are presented in Sec. 4. Throughout this work we assumed a standard cosmological model with $\Omega_\Lambda = 0.7$, $\Omega_m = 0.3$, and $H_0 = 70$ km s^{-1} Mpc^{-1}.

2. SAMPLES AND METHODS

In order to correct the RL relation by the accretion rate effect, we will perform a multivariate linear regression fitting considering the luminosity at 5100Å (L_{5100}), Hβ time delay (τ_{obs}) and R$_{\mathrm{CaT}}$ given by:

$$\tau_{\mathrm{obs}} = \alpha + \beta L_{44} + \gamma \mathrm{R}_{\mathrm{CaT}}, \tag{2}$$

where L_{44} is the L_{5100} in units of $10^{44}\,\mathrm{erg\,s^{-1}}$. The coefficients α, β and γ will be determined using the python packages SKLEARN (Pedregosa et al., 2011) and STATSMODELS (Seabold & Perktold, 2010). We will use two samples which are described below.

- Sample 1. We will consider Du & Wang (2019) sample, which reports the L_{5100}, R$_{\mathrm{FeII}}$ and τ_{obs} for 75 Hβ reverberation mapped objects at $z < 0.2$. Then, using Eq. 1, we will get the R$_{\mathrm{CaT}}$ values and obtain the multilinear relation. We expect to find a similar correction to one obtained by Du & Wang (2019).

- Sample 2. We only identified 13 sources with Hβ time lags and independent R$_{\mathrm{CaT}}$ measurements, which belong to the CaFe sample with originally 58 sources (Panda et. al. 2020). The CaFe sample includes an up-to-date compilation of observations with both optical Fe II and NIR Ca II measurements. An extensive description of the sample is included in Panda et al. (2020) and Martínez-Aldama et al. (2021). Times delays were collected from the literature. Although the number of sources is smaller with respect to the previous sample, the 13 sources cover a wide range of L_{5100}, τ_{obs} and R$_{\mathrm{CaT}}$, which is suitable for the presented analysis.

Black hole masses were estimated from the classical RL relation (Bentz et al. 2013), and the Eddington ratio throughout the definition $L_{\mathrm{bol}}/L_{\mathrm{Edd}}$, where $L_{\mathrm{bol}}= 40 \left(\frac{L_{5100}}{10^{42}} \right)^{-0.2}$ (Netzer 2019) and $L_{\mathrm{Edd}} = 1.5 \times 10^{38} \left(\frac{M_{BH}}{M_\odot} \right)$.

3. RESULTS

In order to justify the inclusion of R$_{\mathrm{FeII}}$ and R$_{\mathrm{CaT}}$ in a multilinear regression fitting with L_{5100} and τ_{obs}, it is required at first to show the correlation between the Eddington ratio, R$_{\mathrm{FeII}}$ and R$_{\mathrm{CaT}}$, respectively (Figure 1). For Sample 1 the correlation in both cases is strong considering the Spearman correlation coefficients (ρ) and the $p-$values ($\rho = 0.66$, $p = 2.2 \times 10^{-10}$). Since R$_{\mathrm{CaT}}$ was determined from R$_{\mathrm{FeII}}$ and their uncertainties are not considered in the estimation of the statistical parameters, ρ and $p-$values are the same in both correlations. On the other hand, due to the small number of sources in Sample 2, the $L_{\mathrm{bol}}/L_{\mathrm{Edd}}$-R$_{\mathrm{FeII}}$ relation is weak ($\rho = 0.32$, $p = 0.28$). However, R$_{\mathrm{FeII}}$ values are not used in the presented analysis since the R$_{\mathrm{CaT}}$ is estimated independently. We only show them as a reference of the R$_{\mathrm{FeII}}$ behavior in Sample 2. The correlation coefficient ($\rho = 0.54$) shows a strong corelation in the $L_{\mathrm{bol}}/L_{\mathrm{Edd}}$-R$_{\mathrm{CaT}}$ relation, although the p-value ($p = 0.058$) indicates a $\sim 5\%$ to reject the correlation. As Martínez-Aldama et al. (2021) pointed out, the correlations with respect to the Eddington ratio are better represented by R$_{\mathrm{CaT}}$ than R$_{\mathrm{FeII}}$. This result was the motivation to use R$_{\mathrm{CaT}}$ instead of R$_{\mathrm{FeII}}$ to correct the RL relation by the accretion rate effect.
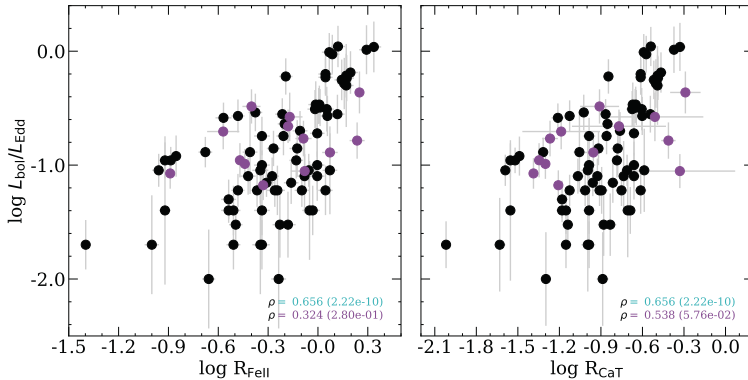
Figure 1: Correlation between the Eddington ratio as a function of R_{FeII} (left panel) and R_{CaT} (right panel), respectively. Cyan and magenta symbols correspond to Sample 1 and 2, respectively (See Sec. 2). The Spearman rank coefficients and the p–values are reported for each case.

The top panels of Figure 2 show the results for the 75 objects from Sample 1. The top-left panel shows the classical RL relation. The color bar represents the R_{CaT} strength, where the strongest R_{CaT} values show the largest departures from the classical RL relation, which is reflected in the large scatter, $\sigma \sim 0.299$ dex. The departure can be estimated by the parameter $\Delta\tau_{obs} = \tau_{obs} - \tau_{RL}$. The inset panel clearly shows the correlation between $\Delta\tau_{obs}$ and R_{CaT} and justifies the inclusion of R_{FeII} in the multilinear relation. Meanwhile, the top-right panel shows the multilinear RL relation including the R_{CaT} where the scatter decreases by almost 1 dex ($\sigma \sim 0.204$). If we compared our relation with the one reported by Du & Wang (2019, $\tau_{obs} = (1.65 \pm 0.06) + (0.45 \pm 0.03)L_{44} + (-0.35 \pm 0.08)R_{FeII}$), both relations are equivalent within uncertainties, since we are using the Eq. 1 to get the values of R_{CaT}. There are small variations in the coefficients and the scatter (0.204 vs. 0.196), however, this does not represent a significant change.

The bottom panels of Figure 2 show the results from the 13 sources with Hβ time delays and independent R_{CaT} estimations (Sample 2). Bottom-left panel shows the classical RL relation with a scatter of $\sigma = 0.289$ dex. The departure parameter $\Delta\tau_{obs}$ from the classical RL relation is not so clear, such as the inset panel with the $\Delta\tau_{obs}$–R_{CaT} relation shows. Although the correlation coefficient ($\rho = 0.44$) shows a moderate correlation between R_{CaT} and $\Delta\tau_{obs}$, the p-value indicates a probability of $\sim 13\%$ to reject the correlation. The bottom-right panel shows the multilinear RL relation with a reduction in the scatter by almost 1 dex, similar to the results for Sample 1. If we compare this correlation with the one obtained from Sample 1 (top-right panel), we find a significant variation in the coefficients. The coefficient associated with L_{5100} is shallower than the one obtained previously (0.39 vs. 0.46). The coefficient associated with the R_{CaT} parameter has a large uncertainty ($\sim 78\%$), which is due to the large uncertainties of R_{CaT} and the weak relation between $\Delta\tau_{obs}$ and R_{CaT}.
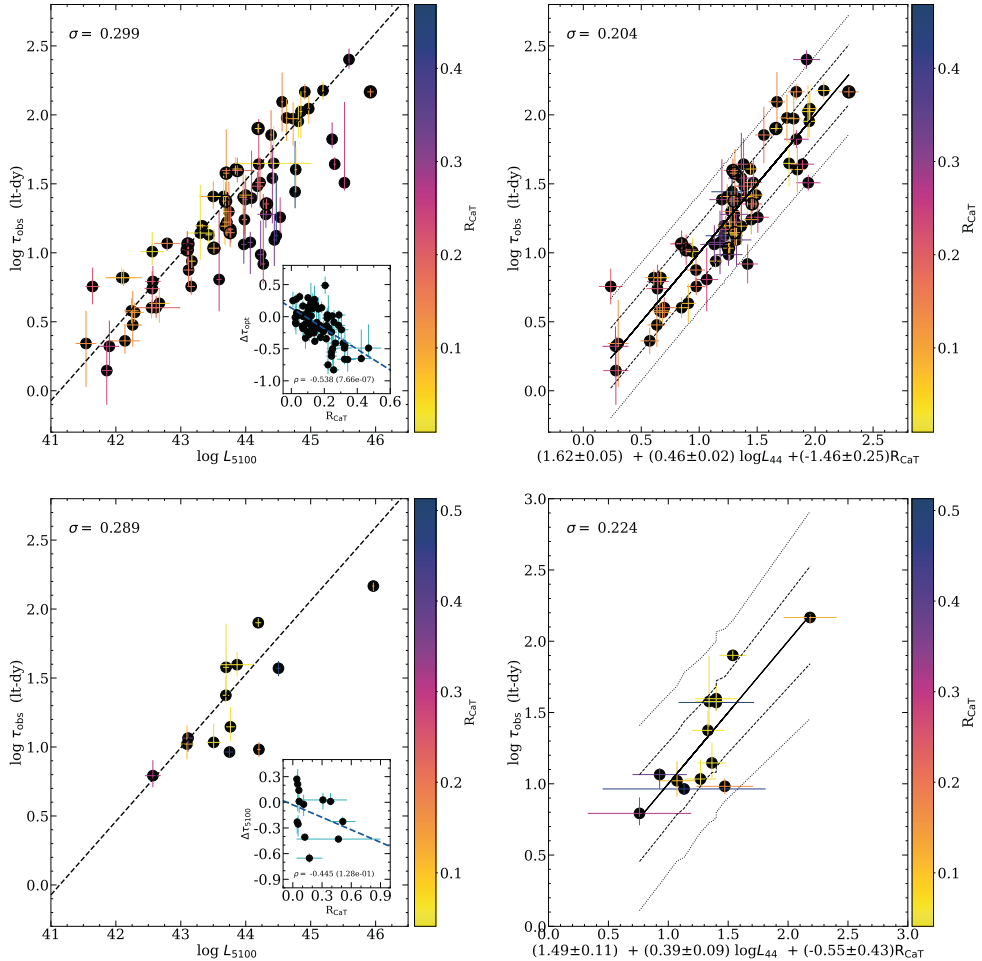
Figure 2: TOP-LEFT PANEL: RL relation using the 75 sources from Du & Wang (2019) sample. TOP-RIGHT PANEL: Multilinear RL relation including the R_{CaT}. Inset plot represents the correlation between $\Delta\tau_{obs}$ and R_{CaT} where the blue dashed lines indicate the best fits. In both panels in the top row, black circles correspond to 10 out of the 13 sources considered in Sample 2 (See Section 2). BOTTOM-LEFT PANEL: RL luminosity relation using the 13 sources from Sample 2. BOTTOM-RIGHT PANEL. Multilinear RL relation including R_{CaT}. In all the panels the color code indicates the R_{CaT} strength. Black dashed lines in the left panels indicate the classical RL relation from Bentz et al. (2013). In the right panels, the black continuous line marks the multidimensional RL relation, while dashed and dotted lines denote the 68% and 95% confidence intervals.

4. DISCUSSIONS AND CONCLUSIONS

We performed a multilinear relation with L_{5100}, τ_{obs} and R_{CaT} in order to recover the classical RL relation (Bentz et al. 2013). Due to the large numbers of sources

in Sample 1, the multilinear RL relation has a better approximation to the classical result (Bentz et al., 2013). Since R_{CaT} measurements were estimated from the R_{FeII}, the relation is so similar to the one obtained from Du & Wang (2019). On the other hand, we could only identify 13 sources with independent measurements of R_{CaT} that are reverberation-mapped. Although the number of sources is small, this second option provides an independent test and will predict better results once the source count increases. In both cases, we achieved to decrease the scatter, however the uncertainties of the coefficients in Eq. 2 are still large for Sample 2. Observing the NIR spectrum in sources already analyzed by the reverberation mapping technique is required in order to improve our results and confirm the Ca II triplet as a proxy of the Eddington ratio with a higher significance.

In results of Sample 1 and 2, the coefficient associated with L_{5100} is shallower than the predicted ($\log \tau_{obs} \propto 0.5 \log L$) by the photoionization theory, theoretical models (e.g. Czerny & Hryniewicz, 2011) and the standard RL relation (Bentz et al. 2013). On the other hand, the independent coefficient in the classical RL relation is given by 1.527 ± 0.31. In our predictions the independent coefficients are in agreement within uncertainties ($\alpha_{S1} = 1.62 \pm 0.05$, $\alpha_{S2} = 1.46 \pm 0.09$). Therefore, we can conclude that the presented multilinear RL relations are in agreement within uncertainties. Some theoretical models have included a shielding effect and a variation in the accretion rate, which shortens the time delay (Naddaf et al. 2021a,b). However, a variation in the slope of L_{5100} is still not included. In the future, these theoretical results will provide the shape of the line profiles and their dependence on the accretion rates. So, it will be a test for the results presented in this paper.

Acknowledgements

References

Bentz, M. C., Denney, K. D., Grier, C. J. et al.: 2013, ApJ, **767**, 149.
Boroson, T. A. and Green, R. F.: 1992, ApJS, **80**, 109.
Czerny, B. and Hryniewicz, K.: 2011, A&A, **525**, L8.
Dalla Bonta, E., Peterson, B. M., Bentz, M. C. et al.: 2020, arXiv:2007.02963.
Du, P. and Wang, J.-M.: 2019, ApJ, **886**, 42.
Du, P., Zhang, Z.-X., Wang, K. et al.: 2018, ApJ, **856**, 6.
Du, P., Hu, C., Lu, K.-X. et al.: 2015, ApJ, **806**, 22.
Ferland, G. J. and Persson, S. E.: 1989, ApJ, **347**, 656.
Fonseca Alvarez, G., Trump, J. R., Homayouni, Y. et al.: 2020, ApJ, **899**, 73.
Dultzin, D., Marziani, P., de Diego, J. A. et al.: 2020, FrASS, **6**, 80.
Joly, M.: 1989, A&A, **208**, 47.
Martínez-Aldama, M. L., Panda, S., Czerny, B. et al.: 2021, submitted to ApJ, arXiv:2101.06999.
Martínez-Aldama, M. L. Zajaček, M., Czerny, B. and Panda, S.: 2020, ApJ, **903**, 2.
Martínez-Aldama, M. L., Czerny, B., Kawka, D. et al.: 2019, ApJ, **883**, 170.
Martínez-Aldama, M. L., Dultzin, D., Marziani, P. et al.: 2015, ApJS, **217**, 3.
Marinello, M., Rodríguez-Ardila, A., García-Rissmann, A. et al.: 2016, ApJ, **820**, 116.
Marziani, P., Zamanov, R. K., Sulentic, J. W. and Calvani, M.: 2003, MNRAS, **345**, 1133.
Naddaf, M.-H., Czerny, B. and Szczerba, R.: 2021a, submitted to ApJ, arXiv:2102.00336.

Naddaf, M.-H., Czerny, B. and Szczerba, R.: 2021b, *XXXIX Polish Astronomical Society Meeting*, **10**, 279.

Netzer, H.: 2019, MNRAS, **488**, 4.

Onoue, M., Banados, E., Mazzucchelli, C. et al.: 2020, ApJ, **898**, 105.

Panda, S., Czerny, B., Adhikari, T. P. et al.: 2018, ApJ, **866**, 115.

Panda, S., Martííez-Aldama, M. L., Marinello, M. et al.: 2020, ApJ, **902**, 76.

Panda, S.: 2021, submitted to A&A, arxiv:2004.13113.

Pedregosa, F., Varoquaux, G., Gramfort, A. et al.: 2011, *Journal of Machine Learning Research*, **12**, 2825.

Persson, S. E.: 1988, ApJ, **330**, 751.

Peterson, B. M., Wanders, I., Bertram, R. et al.: 1998, ApJ, **501**, 82.

Planck Collaboration, Aghanim, N., Akrami, Y. et al.: 2020, A&A, **641**, A6.

Riess, A. G., Casertano, S., Yuan, W. et al.: 2018, ApJ, **861**, 126.

Risaliti, G. and Lusso, E.: 2019, *Nature Astronomy*, **3**, 272.

Sánchez, P., Lira, P., Cartier, R. et al.: 2017, ApJ, **849**, 110.

Seabold, S. and Perktold, J.: 2010, *Proceedings of the 9th Python in Science Conference*, Ed. Stéfan van der Walt and Jarrod Millman, 92–96.

Shen, Y. and Ho, L. C.: 2014, *Nature*, **513**, 210.

Yu, L.-M., Bian, W.-H., Wang, C. et al.: 2019, MNRAS, **488**, 1519.

Zajaček, M., Czerny, B., Martínez-Aldama, M. L. et al.: 2021, submitted to ApJ, arXiv:2012.12409.